Earthq Eng & Eng Vib (2021) 20: 645-660 **DOI**: https://doi.org/10.1007/s11803-021-2044-5

Static and dynamic inelastic *P*–Δ effect for seismic design

Li Xiao† and Tong Genshu‡

Department of Civil Engineering, Zhejiang University, Hangzhou 310058, China

Abstract: Seismic influence of *P*–Δ effect is the subject of this study. First, it is pointed out that the elastic static amplification factor shall be isolated in formulating the dynamic inelastic second order effect. An amplification factor for the static inelastic *P*–Δ effect is derived. Seismic force reduction factors (SFRF) for given ductility and stability coefficients are computed for one-story, one-span frames. The *P*–Δ amplification factors for seismic base shears are obtained by dividing SFRFs with and without *P*–Δ effect. Both *P*–Δ amplification factors and SFRFs are presented separately with two kinds of period abscissas. The *P*–Δ amplification factors are dependent on periods with the maximum occurring at about 0.75 s for site type C and approach to the static inelastic counterpart at long periods. Post-yield stiffness cannot fully counteract the adverse impact of the *P*–Δ effect. Formulas for seismic *P*–Δ amplification factors are proposed and compared to results of others. Collapse capacity spectra (CCS) are reviewed and their application in codes discussed. Available CCSs are compared with SFRFs with finite ductility computed for two ensembles of seismic records. A comparison reveals that the SFRFs are affected by seismic records, and available CCSs do not always provide upper limits for the SFRFs when stability coefficients are greater than 0.1 for frame models.

Keywords: seismic force reduction factor; *P*–Δ effect; amplification factor; dynamic stability; characteristic period

1 Introduction

The $P-\Delta$ effects reduce the lateral resistance of structures. Under the effect of strong earthquakes, structures experience severe inelastic deformation, and the $P-\Delta$ effect may cause partial or total loss of load carrying capacity. Many studies on the influence of the $P-\Delta$ effect on seismic demand have been carried out (Gupta and Krawinkler, 2000; Adam and Jäger, 2012; Rosenblueth, 1965; Bernal, 1987), but because of the inherent complexity of the seismic response of buildings, this topic still attracts the attention of researchers in this time-consuming area.

1.1 Second order effect in the stability check of columns

The $P-\Delta$ effect in static elastic cases is quantified by the stability coefficient computed by:

$$\theta_{\mathrm{e}}=\frac{P_{\mathrm{Ed}}}{P_{\mathrm{cr}}} \tag{1}$$

where P_{Ed} is the design load on the structure and P_{cr} is the elastic buckling load for global instability based on initial elastic lateral stiffness. For a non-seismic design, $P-\Delta$ effect is included either in the strength check of columns in terms of the moment amplification factor in the form:

$$A_{\mathrm{e}}=\frac{1}{1-\theta_{\mathrm{e}}} \tag{2}$$

and the effective length of a column or through the second-order elastic analysis and the system length of columns.

For seismic design, the $P-\Delta$ effect cannot be described by Eq. (2) because of large inelastic lateral deformation involved in the seismic design philosophy. To accommodate this increased second order effect, Rosenblueth (1965) proposed the following seismic force amplification factor (SFAF):

$$A_{\mathrm{Rosenblueth}}=\frac{1}{1-\mu\theta_{\mathrm{e}}} \tag{3}$$

where μ is the ductility factor. Eurocode 8 (CEN, 2005) adopts Eq. (3) to amplify the seismic action effects.

Based on clause 4.4.2.2 of Eurocode 8, the equation for the in-plane buckling strength of a beam-column would be as follows:

$$\frac{P_G+\dfrac{P_E}{1-\mu\theta_{\mathrm{e}}}}{\chi P_P}+\frac{M_G+\dfrac{M_E}{1-\mu\theta_{\mathrm{e}}}}{(1-\theta_{\mathrm{e}})M_P}\le 1 \tag{4}$$

Correspondence to: Tong Genshu, Department of Civil Engineering, Zhejiang University, Hangzhou 310058, China
Tel: +86-571-8795-2259
E-mail: tonggs@zju.edu.cn
†PhD Candidate; ‡Full Professor
Received September 19, 2019; **Accepted** May 13, 2020

where P_G and M_G are the axial force and bending moment due to gravitational loads, respectively; P_E and M_E are the axial force and bending moment due to the design level seismic action, respectively; χ is the strength reduction factor of column due to buckling, as specified in Eurocode 3 Part 1.1; and P_P is the yield strength of the steel cross-section.

Equation (4) seems strange because the earthquake moment M_E is amplified twice. To avoid this, the static elastic $P-\Delta$ amplification factor $1/(1-\theta_e)$ shall be isolated from the total inelastic amplification factor as follows:

$$\frac{A_F}{1-\theta_e} \tag{5}$$

A_F is the inelastic seismic $P-\Delta$ amplification factor for the seismic action to be sought in this study.

1.2 Literature review of the inelastic dynamic second-order effect

Bernal (1987) carried out a study on the inelastic dynamic $P-\Delta$ effect; four records were used, and the seismic force amplification factors (SFAF) due to the $P-\Delta$ effect were calculated at 37 periods that were evenly spaced between 0.2 and 2.0 s. The following equation was proposed for the SFAF:

$$A_{F,\text{Bernal}} = \frac{1+1.87(\mu-1)\theta_e}{1-\theta_e} \tag{6}$$

It would be applied with first order elastic analysis.

Wei *et al*. (2012) reported an investigation of the $P-\Delta$ amplification factor of the ideal bilinear elastic-plastic model, with 308 ground motions recorded on site classes B, C, and D. Analysis was carried out over the course of 8 periods: 0.25, 0.5, 0.75, 1, 1.5, 2, 2.5 and 3 s. Data was processed with θ_e and $\mu\theta_e$ as the abscissa respectively, and Eq. (7) was proposed for the SFAF based on the statistical mean values:

$$A_{F,\text{Wei}} = 1.05 + \left(2 - \frac{1}{e^{0.85(\mu-1)}}\right)\mu\theta_e \tag{7}$$

Amara *et al*. (2014) carried out a similar study to that of Wei *et al*. (2012) using two ensembles, each containing 20 seismic records, and the periods ranged from 0.15 to 2.0 s with step 0.01. The values were averaged for each combination of (θ_e, μ); thus the effect of periods was eliminated. The proposed SFAF equations were the smallest among available results for similar research studies.

As reported in MacRae (1994), Neuss *et al*. (1983) recommended the use of expected inelastic drift to compute the $P-\Delta$ bending moment. This method was further developed by Priestley *et al*. (1993) and was applied in the displacement-based seismic design done by Priestley *et al*. (2007). The New Zealand Seismic code (NZS 1170.5., 2004) requires the $P-\Delta$ effect to be computed using inter-story inelastic drift at the ultimate limit state, and the inelastic second-order moment should not be larger than 0.3 times the bending moment due to the design level seismic shear force.

Besides Eq. (6), Bernal (1987) also suggested a limit on the maximum applicable ductility, based on the load-carrying demand of buildings in the post-earthquake stage:

$$\mu_{\text{limit}} = \frac{C}{\theta_e}, C=0.4 \tag{8}$$

i.e., the ductility capacity of a frame may be greater than μ_{limit}, but only a smaller value equal to μ_{limit} is allowed to be used. A similar criterion has been incorporated into the ASCE 7 (2010) since 1993 (UBC 93) in a converted form:

$$\theta_{e,\text{lim}} = \frac{0.5}{\beta C_d} \tag{9}$$

in which C_d is the drift amplification factor that accounts for inelastic deformation, β is the ratio of shear demand to shear capacity and is permitted to be taken as 1 ($1/\beta$ can be understood as an overstrength factor). Based on the load and resistance factors applied in the Eurocodes, Asimakopoulos *et al*. (2007) suggested $C = 0.55$ in Eq. (8).

1.3 Review of the collapse capacity spectrum

More recently, a collapse capacity spectrum (CCS) was introduced. Miranda and Akkar (2003) defined the collapse capacity spectral value as the value of R_c, at which the bilinear elastic-plastic system with negative post-yield stiffness has a sudden increase of drift as R shows only a small increase; here, R is defined by:

$$R = \frac{mS_a}{F_y} \tag{10}$$

in which m is the mass of the oscillator, S_a is the elastic acceleration spectrum, and F_y is the yield strength of the elastic-plastic system. R_c varies with periods and post-yield stiffness, Miranda and Akkar (2003) analyzed systems with periods ranging from 0.2 to 3.0 s while subjected to 72 earthquake ground motions from firm soil, and proposed Eq. (11) for the mean (greater than median) spectra of R_c:

$$R_c = 1 + \left(1 - \frac{1}{e^{7.5T}}\right)\frac{0.26}{(\theta_e-\alpha)^{0.89+0.04T+0.15\ln T}} \tag{11}$$

where T is the period, and α is the post-yield stiffness ratio. Equation (11) is independent of the ductility factor

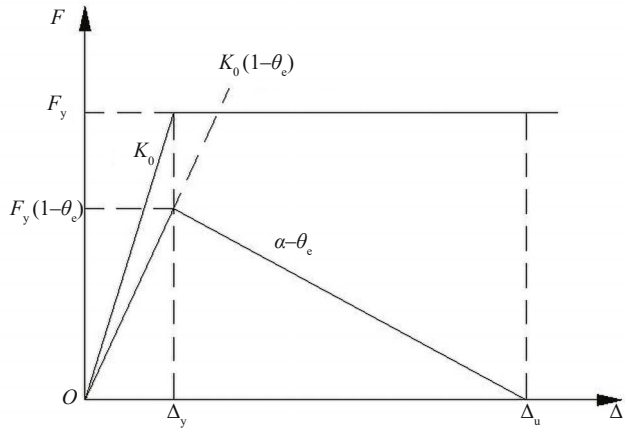

Fig. 1 Bilinear model with and without *P*-Δ effect

because Miranda and Akkar (2003) adopted a bilinear elastic-plastic relation (Fig. 1). The only limitation on the post-yield branch is the zero lateral strength after the drift reaches Δ_u where:

$$\Delta_u = \frac{F_y}{K_0} + \frac{F_y}{(\theta_e - \alpha)K_0} = \left(1 + \frac{1}{\theta_e - \alpha}\right)\Delta_y \tag{12}$$

FEMA 440 (2005) presented Eq. (13) for the CCS, which is rather close to, Eq. (11):

$$R_c = 1 + \frac{0.25}{(\theta_e - \alpha)^{1+0.15\ln T}} \tag{13}$$

Adam and Jäger (2012) made a similar investigation regarding the CCS. The ATC63 far-field (ATC63-FF) 44 seismic records on NEHRP (FEMA-368, 2000) site classes C (soft rock) and D (stiff soil) were used. The following CC median spectra were proposed for the bilinear hysteretic model:

$$R_c = \begin{cases} \dfrac{2}{3(\theta_e-\alpha)^{2/3}} T^{0.01+\frac{0.03}{(\theta_e-\alpha)^{0.7}}} & T \le T_1 \\ \dfrac{2}{3(\theta_e-\alpha)^{2/3}}\left[T_1^{0.01+\frac{0.03}{(\theta_e-\alpha)^{0.7}}} + \left(0.01+\dfrac{0.03}{(\theta_e-\alpha)^{0.7}}\right) T_1^{\frac{0.03}{(\theta_e-\alpha)^{0.7}}-0.99}(T-T_1)\right] & T > T_1 \end{cases} \tag{14a}$$

where

$$T_1 = \min\left[3.6,\ 40(\theta_e - \alpha) - 0.4)\right] \tag{14b}$$

Adam and Jäger (2012) also found that the median CCSs for the Peak-oriented and pinching hysteretic models are slightly greater than CCSs for bilinear models. Eq. (11) is significantly greater than Eq. (14) when the period is longer than 2.5 s.

Equation (8) specifies the maximum ductility factor permitted to be utilized. Similarly, Eq. (11) or Eq. (14a) may be used. Even if the ductility is infinite, the strength reduction factor is limited by Eq. (11) or by Eq. (14). Considering that the ductility definition always includes the elastic part of the system, i.e., the ductility factor is never less than 1.0, instead of Eq. (8), the following equation was proposed:

$$R_c = \mu_c = 1.0 + \frac{C_{A\&J}}{\theta_e - \alpha} \tag{15a}$$

and because Eq. (14) is used as a reference for the simplification, one obtains

$$C_{A\&J} = 0.156 + (0.051 - 0.135\theta_e)T \tag{15b}$$

$C_{A\&J} = 0.178 - 0.332$ when $T = 0.5 - 4$ s. A comparison of Eq. (15) with Eq. (14) is given in Fig. 2. Equation (8) is also shown in Fig. 2(a). From this comparison,

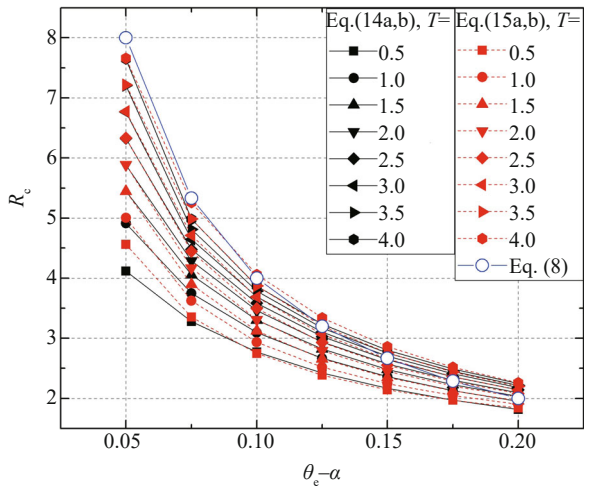

(a)

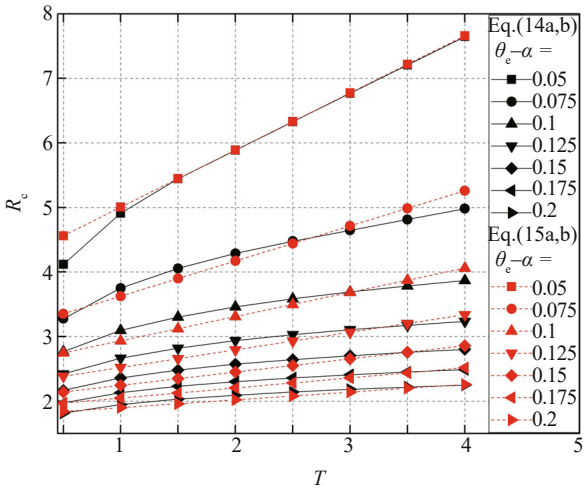

(b)

Fig. 2 Comparison of Eq. (14) and Eq. (15)

one may understand that the application of Eq. (14) is similar to Eq. (8), but they are from different derivations. Equation (14) is fundamentally important.

Ibarra and Krawinkler (2005) carried out a comprehensive study on CCSs with limited ductility. They used backbone curves composed of three linear segments: linear elastic (stiffness K, yield drift δ_y), post-yield hardening (stiffness $\alpha_s K$, the capping drift δ_c) and a post-capping segment with a negative slope $-\alpha_c K$. Three types of hysteretic curves (bilinear, peak-oriented and pinching models) were used, and 40 seismic records (LMSR-N) from California were adopted to construct the CCSs. The ratio δ_c/δ_y is set to be 2, 4 and 6, respectively, representing high, medium and low ductility systems. The post-capping stiffness parameter α_c is set to 0.1, 0.3 and 0.5, modeling small, as well as steep and very steep reduction of the post-capping capacity. The $P-\Delta$ parameter is set to be 0.0, $0.0178T$ and $0.0356T$, where T is the period. By using such detailed hysteretic models, the ratio δ_c/δ_y, the post-capping stiffness α_c and the $P-\Delta$ effect were identified to be the three parameters that most influence the collapse capacity of a system. Cyclic deterioration is an important but not dominant issue for collapse evaluation. $P-\Delta$ effects greatly accelerated collapse of deteriorating systems and may be the primary source of collapse for flexible but very ductile structural systems. Ibarra and Krawinkler (2005) also revealed that under the same δ_c/δ_y, ratio systems with small negative post-capping stiffness have significantly larger collapse capacity than those with large or very large negative stiffness.

For models with steep and very steep post-capping negative stiffness, the CCS of Ibarra and Krawinkler (2005) for a given ratio δ_c/δ_y is close to the spectrum of seismic force reduction factors (defined by Eq. (10)) of others (Miranda and Bertero, 1994; Borzi and Elnashai, 2000) for a prescribed ductility $\mu = \delta_c/\delta_y$ beyond which the system is regarded as being fully collapsed, i.e., including the post-capping segment with steep and very steep negative stiffness in determining R leads only to a small increase in R when compared with fully neglecting the post-capping negative segment.

CCSs represent the upper limits for assessing the seismic behavior of existing building. For new buildings, the $P-\Delta$ effect is preferably included in advance in the determination of the seismic base shear, and if doing so, the probability of collapse will be minimal. The stability coefficient θ_e is not solely determined by the period (Ibarra and Krawinkler, 2005), so in this paper θ_e is regarded as an independent parameter in the determination of the seismic force amplification factor (denoted by A_{F,θ_e} or $A_{\mu\theta}$), accounting for the inelastic $P-\Delta$ effect.

It might be appropriate here to mention that Bernal (1992) is the first to propose the collapse spectrum, but he expressed it via inelastic acceleration spectra which depends on period, stability coefficient and peak ground velocity.

Borekci *et al*. (2014) studied the collapse spectra caused by stiffness and strength degradations: no $P-\Delta$ effect was included. Ucar and Merter (2018) adopted energy-based equilibrium equations to include the $P-\Delta$ effect.

1.4 Inelastic spectra of this study

The spectra of the seismic force reduction factor (SFRF) of a system for a prescribed ductility factor have been extensively studied (Miranda and Bertero, 1994; Borzi and Elnashai, 2000). Miranda (1993) introduced a "predominant period of the ground motion", T_{gE}, to normalize the abscissa of the SFRF spectra, R_μ, for soft soil, and T_{gE} is the period at which the peak relative velocity of a 5% damped linear elastic system occurs. It was found to be very close or nearly equal to period T_{gR} at which the peak value of R_μ occurs. Ordaz and Pérez-Rocha (1998) proposed a new R_μ spectrum based on the observation that the maximum SFRF occurs at a period, denoted as T_{gD}, where the spectral displacement was also a maximum. In fact, $T_{gE} \approx T_{gR} \approx T_{gD}$ (Zhao and Tong, 2009).

Denoting the period at which the elastic acceleration has a peak value by T_{ga}, T_{ga} is slightly less than the intersection period ($T_{\mathrm{A/V}}$) of the constant spectral acceleration and constant velocity regions, and T_{gR} was greater than the intersection period ($T_{\mathrm{V/D}}$) of the constant spectral velocity and constant displacement regions of a 5% damped Newmark-Hall type spectrum. Currently the elastic acceleration spectra were expressed in four period subranges: (0, 0.1), $(0.1, T_{\mathrm{A/V}})$, $(T_{\mathrm{A/V}}, T_{\mathrm{V/D}})$ and $(>T_{\mathrm{V/D}})$, and it was realized that the SFRF spectra should be similarly expressed. The SFRF spectra in this paper will be constructed with the period abscissa being divided into 3 ranges: $(0, T_{ga})$, (T_{ga}, T_{gR}) and (T_{gR}, ∞). Correspondingly, the elastic acceleration spectra S_a are also established with the period in three ranges $(0, T_{ga})$, (T_{ga}, T_{gD}) and (T_{gD}, ∞).

In this study, one-story, one-bay frames are adopted. An ensemble of 102 earthquake records on site soil type C from PEER Ground Motion Database and another ensemble of 44 far-field seismic records proposed in FEMA-P695 are used in this analysis. The 102 and 44 spectral values for several specific periods are checked to reveal their probabilistic distribution. Dynamic inelastic $P-\Delta$ effect is represented by an amplification factor for the base shear, and the amplification factors are compared with those obtained in a static inelastic $P-\Delta$ analysis. The effect of post-yielding stiffness is studied to check whether the unfavorable effect of the $P-\Delta$ effect is mitigated. The R_μ spectra are constructed with two types of abscissas. Finally, simplified formulae are proposed for the dynamic inelastic $P-\Delta$ effect of SDOF systems.

2 Static *P*–Δ effect in the inelastic stage

Figure 3 shows two drift states of a cantilever: the drift at yielding and the drift at the ductility limit μ. At the drift of the ductility limit, the displacement of the oscillator is the maximum, but its velocity is zero, so one may see it as if it was in a static state; the acceleration is also a maximum and the inertia force is in equilibrium with the physical restoring force of the oscillator. At this state, the maximum second-order base moment is derived as follows.

The elastic lateral stiffness is K_0 (Fig. 1) and the base shear is F_{y0}. Because static elastic second-order analysis is carried out or the second order effect is considered in the member capacity check (ANSI/AISC 360-10), the member′s plastic moment will be:

$$M_{\mathrm{P}} = F_{y0}h + P\Delta_{\mathrm{y}} = \frac{F_{y0}h}{1-\theta_{\mathrm{e}}} \tag{16}$$

where $\theta_{\mathrm{e}} = \dfrac{P}{hK_0}$. Equation (16) represents the transient point between elastic and plastic states. From Eq. (16):

$$P\Delta_{\mathrm{y}} = \frac{\theta_{\mathrm{e}}}{1-\theta_{\mathrm{e}}}F_{y0}h \tag{17}$$

And after it yields at the base shear force F_{y0}, it flows plastically to the ductility limit; the total displacement is $\mu\Delta_{\mathrm{y}}$. At this displacement point there is no damping force because of zero velocity, so the bending moment at the base is:

$$M_{\max} = F_{y0}h + P\cdot\mu\Delta_{\mathrm{y}} = \left(1+\frac{\mu\theta_{\mathrm{e}}}{1-\theta_{\mathrm{e}}}\right)F_{y0}h = \frac{1+\theta_{\mathrm{e}}(\mu-1)}{1-\theta_{\mathrm{e}}}F_{y0}h = \left[1+\theta_{\mathrm{e}}(\mu-1)\right]M_P > M_P \tag{18}$$

Because of $M_{\max} > M_P$, the system will lose its dynamic stability. To avoid dynamic instability, one should amplify the required capacity in advance. Based on Eq. (18), the base shear amplification factor should be:

$$A_{F,\mathrm{static}} = 1+\theta_{\mathrm{e}}(\mu-1) \tag{19}$$

The amplified base shear is now:

$$\left[1+\theta_{\mathrm{e}}(\mu-1)\right]F_{y0}$$

correspondingly the bending moment based on static elastic second order analysis is amplified to Eq. (18), and therefore dynamic instability can be avoided.

One may also interpret Eq. (19) in a different way: if a structure is designed without considering an amplified inelastic $P-\Delta$ effect, then to assure the stability of the structure in a severe seismic event, the overstrength factor should be at least as large as Eq. (19).

Equation (19) is derived statically. In the following section, inelastic dynamic analysis will be carried out to check whether Eq. (19) is also valid under the action of real seismic records.

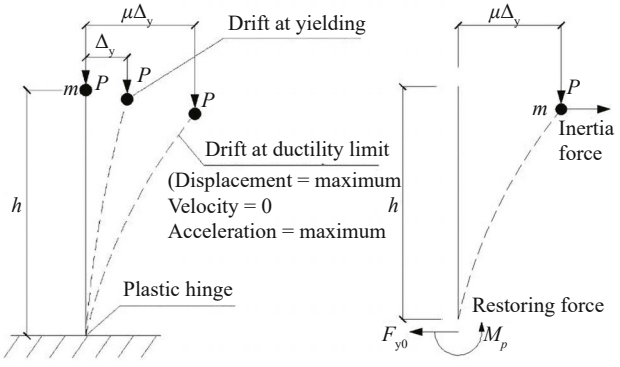

Fig. 3 Drifts at yielding and the ductility limit

3 Dynamic *P*–Δ effect in the inelastic system

In determining the R_μ spectra, elastic dynamic analysis is first carried out to find the maximum base force $F_{\mathrm{e,max}}$, and then inelastic dynamic analysis is carried out to find the inelastic base shear $F_{\mathrm{y},\mu}$ for a prescribed system ductility factor μ, finally $R_\mu = F_{\mathrm{e.max}} / F_{\mathrm{y},\mu}$. For each seismic record, the elastic acceleration spectrum S_a has a peak value at T_{ga}, while the R_μ spectrum has a peak value at T_{gR}, where T_{ga} and T_{gR} are computed through linear and elastic-plastic dynamic analyses, respectively. Two spectra (S_a and R_μ) are used to obtain the base shear S_a/R_μ. The period abscissa is divided into three ranges: (0, T_{ga}), (T_{ga}, T_{gR}) and > T_{gR}. Spectral values are outputed at periods $T_i = i\dfrac{T_{ga}}{N_1}$, $T_{ga}+i\dfrac{T_{gR}-T_{ga}}{N_2}$, $T_{gR}+i\dfrac{2T_{gR}}{N_3}$, $i=1,2,....,N_j$, N_j+1, $j=1,2,3$ are the numbers to output spectral values in each period range, and for all seismic records, N_j are the same. Sprectra are constructed by direct summation of spectral values at the same sequence points.

The current available literature constructed spectra of SFRFs for a given site type by providing a direct summation of spectral values in the same period. The present paper will also construct such spectra for comparison.

For SDOF systems, the dynamic equilibrium equation based on the moment at the bottom is:

$$m\ddot{x} + c\dot{x} + [F(k,x) - \theta_{\mathrm{e}}K_0 x] = -m\ddot{x}_{\mathrm{g}} \tag{20}$$

where m is the mass, c is the damping, x is the lateral displacement, $\dot{x}$ and $\ddot{x}$ are the lateral velocity and acceleration, F is the restoring force of the system, and

$\ddot{x}_g$ the seismic acceleration record. The $P-\Delta$ effect is represented by the factor $\theta_e = P/(hK_0)$, P is the axial force, h is the height of the cantilever column, and K_0 is the initial stiffness. The target ductilities are $\mu = 2$, 3, 4, 5, and 6. θ_e are set to be 0, 0.05, 0.1, 0.15 and 0.2.

Additionally, 2D one-bay frames are created by the Open System for the Earthquake Engineering Simulation (OpenSees) structural analysis platform, as illustrated in Fig. 4. The non-yielding members, beams and columns are modelled using elastic beam-column elements because they are capacity-designed and are checked to remain elastic. The columns and beams are W24X104 and W24X68, respectively. The hysteretic behavior of the frame is modelled using zero-length elements at the beam end and column base. The zero-length elements with a material model for steel members (steel01) with a 0.005 post-yield stiffness factor are used to simulate the plastic hinge of the strong-column/weak-beam mechanism. Lumped masses are placed at the nodes. A 5% Rayleigh mass and stiffness proportional damping is adopted. Corotational transformation is utilized to simulate a large nonlinear geometric transformation. The nodes on the same floor are constrained together using equal translational degree-of-freedom.

A flowchart for determing the seismic force reduction factor is shown in Fig. 6 (Qu *et al*., 2011). In the figure, ξ is the damping ratio; F_e is the elastic seismic force; F_y is the yield strength; and Δ_{max} is the maximum drift; Δ_y is the yield drift; μ_{demand} is the demand ductility ; and μ_{target} is the target ductility.

For the ensemble of 102 seismic records, histograms of the R_μ values are presented in Fig. 7 for two periods and $\mu = 2$, the shape of the histograms is close to logarithmic normal distribution.

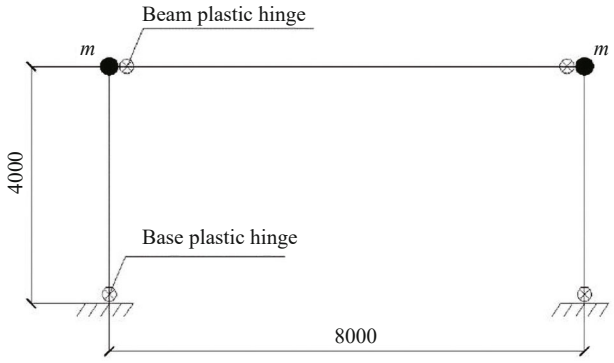

Fig. 4 Two-dimensional one-bay nonlinear analysis frame model (mm)

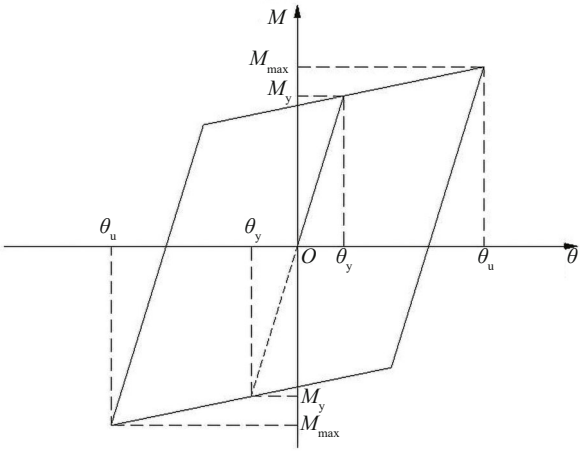

Fig. 5 The hysteresis model of Steel01 for plastic hinges

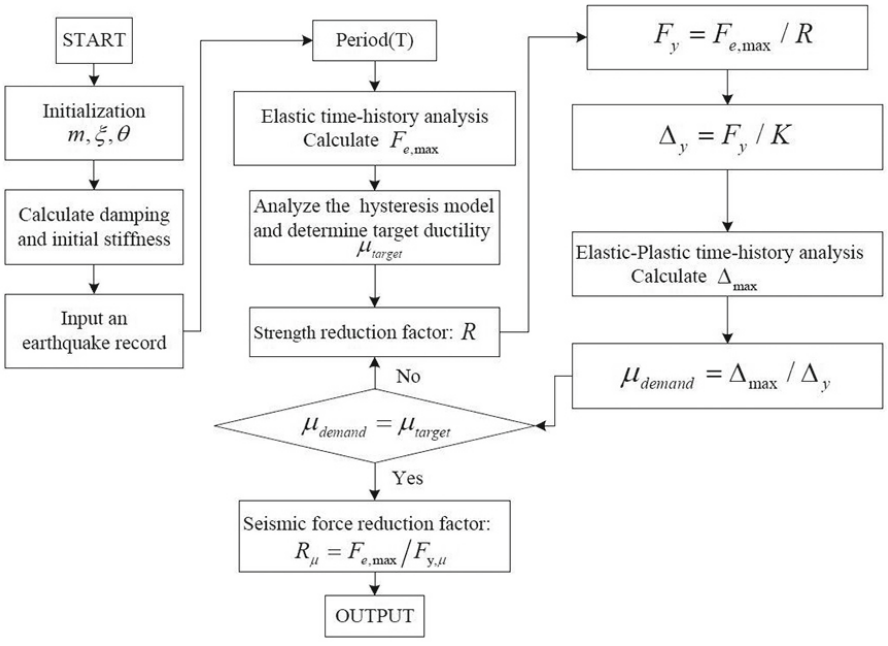

Fig. 6 The flowchart of the iterative procedure for SDOF buildings analysis

The period considering the $P-\Delta$ effect is:

$$T_\theta = 2\pi\sqrt{\frac{m}{K_0 - P/h}} = 2\pi\sqrt{\frac{m}{K_0}\cdot\frac{1}{1-\theta_e}} = \frac{T_{\theta_e=0}}{\sqrt{1-\theta_e}} = \frac{T}{\sqrt{1-\theta_e}} \tag{21}$$

where $T_{\theta_e=0}$ is the period without the $P-\Delta$ effect ($\theta_e = 0$) and will be denoted as T. When $T_\theta = T_{ga}, T_{gR}$, peak points appear on the elastic and inelastic response spectra of the system with the $P-\Delta$ effect, so in the following, the R_μ spectra will be constructed using T_θ / T_{gR} as the abscissa.

The median spectra of the seismic force modification factor for the SDOF building structure is shown in Fig. 8 for $\theta_e = 0,\ 0.05,\ 0.1,\ 0.15,\ 0.2$. Comparing Figs. 8(b)–(e) with Fig. 8(a) ($\theta_e = 0$), it can be seen that:

(1) The SFRFs with the $P-\Delta$ effect are smaller than those lacking the $P-\Delta$ effect, and the larger the $P-\Delta$ factors are, the smaller are the SFRFs;

(2) When the period is less than T_{ga}, R_μ increases rapidly from about 1.0 and reaches the first peak point at T_{ga}. As the period increases to T_{gR}, the spectra reach the second peak point, which is usually larger than the first peak at T_{ga}. For $T > T_{gR}$, the value decreases with the increase of period and flattens gradually after $2T_{gR}$ and tends toward a constant;

(3) The peak values at T_{ga} and T_{gR} drop more quickly than at other periods as the $P-\Delta$ factor increases. Because

$$R_\mu = \frac{F_{e,\theta}}{F_{y,\mu\theta}} = \frac{(K_0 - P/h)\Delta_{e,\theta(\max)}}{(K_0 - P/h)\Delta_{y,\mu\theta}} = \frac{\Delta_{e,\theta(\max)}}{\Delta_{y,\mu\theta}} \tag{22}$$

faster dropping of R_μ implies a quicker increase of $\Delta_{y,\mu\theta}$, where $\Delta_{y,\mu\theta}$ is the yielding displacement for the target ductility, considering $P-\Delta$ effect;

(4) With the increase of θ_e, when $\frac{T_\theta}{T_{gR}} > 1.4$ and $\mu > 3$, the $R_{\mu\theta}$ increases as the period increases, signifying that the influence of the $P-\Delta$ effect is mitigated slightly for longer periods. Note that Eq. (14) expresses the same trend: R_c is larger as the period increases.

The amplification factor of the seismic force due to $P-\Delta$ effect is defined as:

$$A_{F,\mu\theta} = \frac{(1-\theta_e)\times R_{\mu,\theta_e=0}(T/T_{gR})}{R_{\mu\theta}(T_\theta / T_{gR})} \tag{23}$$

where $R_{\mu\theta}$ is defined by Eq. (22). $(1-\theta_e)$ is introduced in Eq. (23) due to the fact that the elastic amplification factor $1/(1-\theta_e)$ will be considered in the member check.

The amplification factor $A_{F,\mu\theta}$ spectra are presented in Fig. 9 for the SDOF system, with a different ductility and $P-\Delta$ effect coefficient. It can be seen that:

(1) $A_{F,\mu\theta}$ is larger as μ becomes larger;

(2) A steep rise of the $A_{F,\mu\theta}$ spectra occurs from 0 to T_{ga};

(3) The values of $A_{F,\mu\theta}$ are the largest at T_{ga} and the second largest at T_{gR};

(4) As the period becomes larger than T_{gR}, $A_{F,\mu\theta}$ drops and it decreases more slowly as the period increases;

(5) In the period range of (T_{ga}, T_{gR}), $A_{F,\mu\theta}$ are smaller than at T_{ga} and T_{gR}.

(6) At the period $3T_{gR}$, $A_{F,\mu\theta}$ is close to $A_{F,\text{static}}$. This is interesting and significant: in the long period range, the static derivation is valid.

Based on Fig. 9, the mean values of the median spectra $A_{F,\mu\theta}$ in the period range of $T_{ga} - T_{gR}$ are computed as follows (Peak points and nearby ranges are not included; the peak values of R_μ in Fig. 8 also are not utilized in practice because of the uncertainty of the characteristic periods):

$$A_{F,\max} = \frac{1}{T_{gR}^- - T_{ga}^+}\int_{T_{ga}^+}^{T_{gR}^-} A_{F,\mu\theta}\,\mathrm{d}T_\theta \tag{24}$$

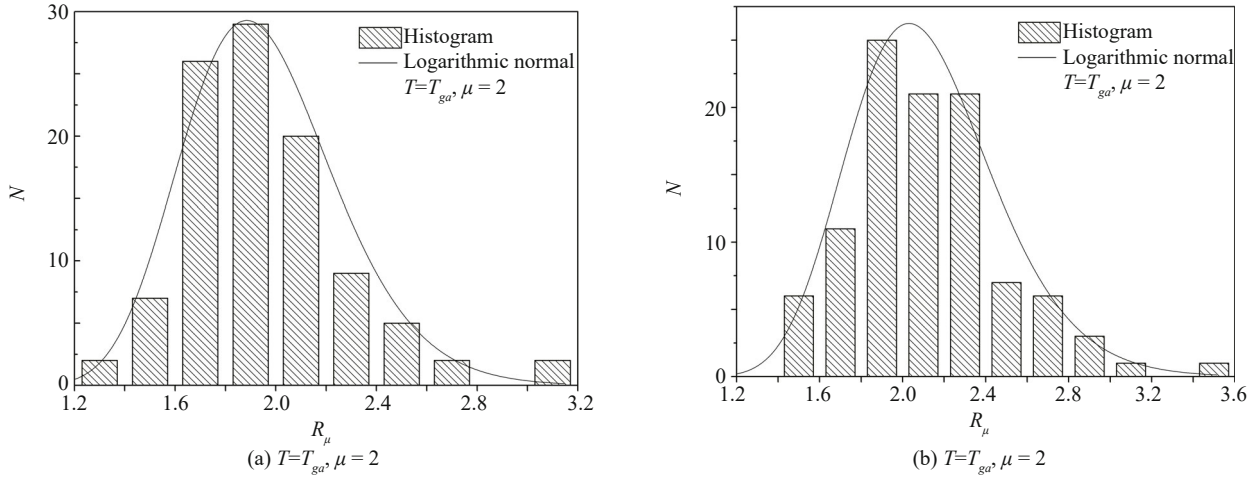

(a) $T=T_{ga}$, $\mu = 2$ (b) $T=T_{ga}$, $\mu = 2$

Fig. 7 Distribution pattern of R_μ value for specific SDOF systems for $\mu = 2$

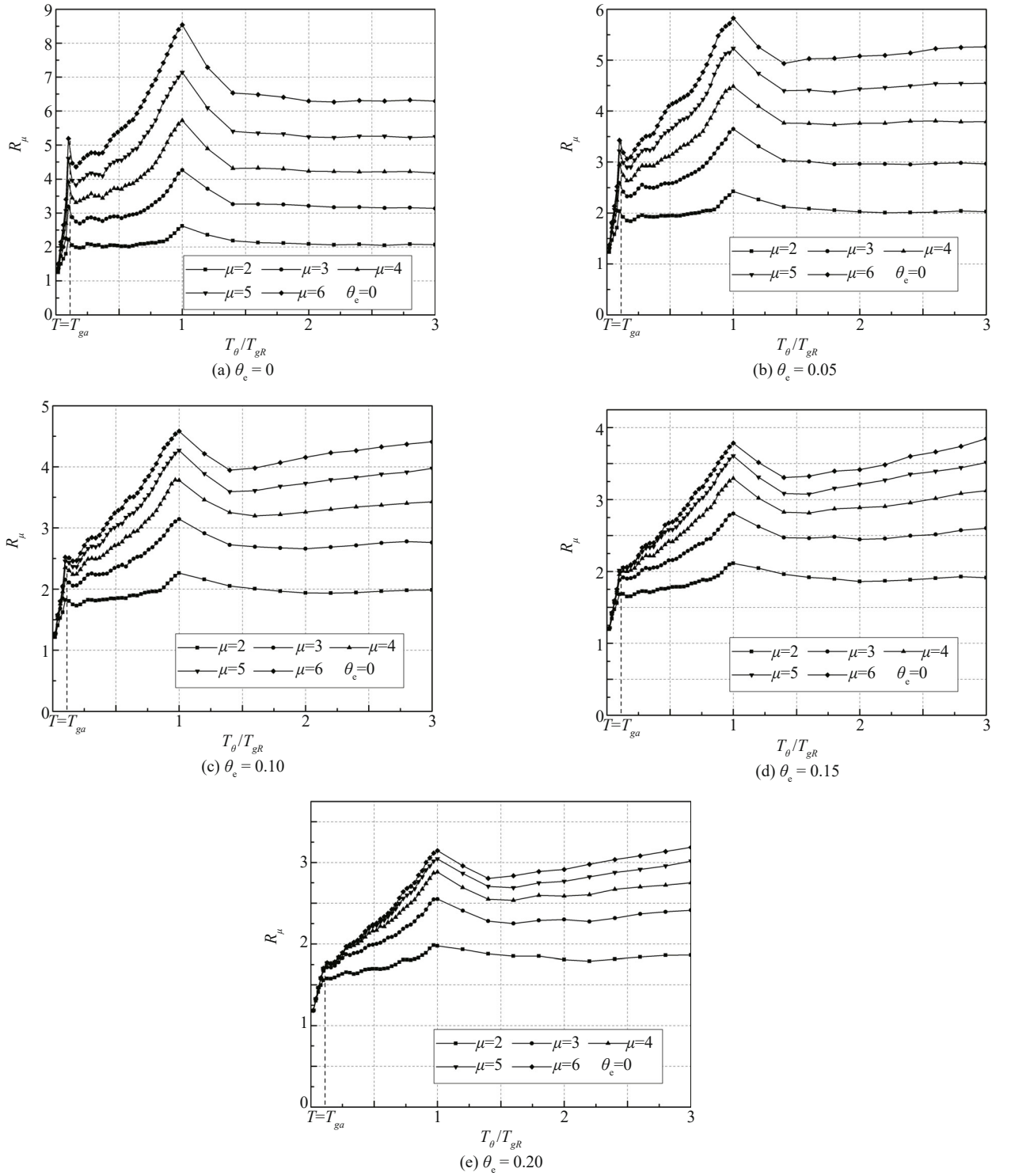

Fig. 8 The median SFRFs spectra for SDOF with frame models

A piecewise function is proposed for the $A_{F,\mu\theta}$ spectra in Fig. 9 as follows:

$$A_{F,\mu\theta}=\begin{cases}1+(A_{F,\max}-1)\dfrac{T_\theta}{T_{ga}} & \left(T_\theta \le T_{ga}\right)\\ A_{F,\max} & \left(T_{ga}<T_\theta \le T_{gR}\right)\\ \left(1-0.01\left(20\theta_e+1\right)\left(\mu-1\right)^{1-1.5\theta_e}\sqrt{\dfrac{T_\theta}{T_{gR}}-1}\right)A_{F,\max} & \left(T_\theta > T_{gR}\right)\end{cases} \tag{25}$$

where

$$A_{F.\max}=1+\left(0.9+0.1\mu\right)\left(\mu-1\right)\theta_e \tag{26}$$

Figure 10 shows a comparison of $A_{F,\text{static}}$ and $A_{F,\max}$. $A_{F,\max}$ has a smaller scatter when the abscissa is taken to be $(\mu-1)\theta_e$ instead of $\mu\theta_e$. $A_{F,\max}$ is larger than $A_{F,\text{static}}$ especially when $(\mu-1)\theta_e$ becomes larger than 0.5.

Therefore, the inelastic dynamic $P-\Delta$ effect is larger than the inelastic static $P-\Delta$ effect in this period range.

An analysis also has been carried out for unlimited ductility, Fig. 11(a) shows the median ductility response $\overline{R}_\mu$ (i.e., Collapse Capacity Spectra of Adam and Jäger (2012)) in the range of $T_{ga}-T_{gR}$ for varied θ_e. It is seen that when $\theta_e > 0$, $\overline{R}_\mu$ has an upper limit due to inelastic dynamic instability. As a comparison, Fig.11 also shows the static ductility response $R_{\mu,\ \text{static}}$, which is based on Eq. (19) and is derived for the period range for which the equal displacement law is valid:

$$R_{\mu,\ \text{static}} = \frac{\mu}{1+\theta_e(\mu-1)} \tag{27}$$

4 Effect of post-yield stiffness

This section will address the issue of whether the

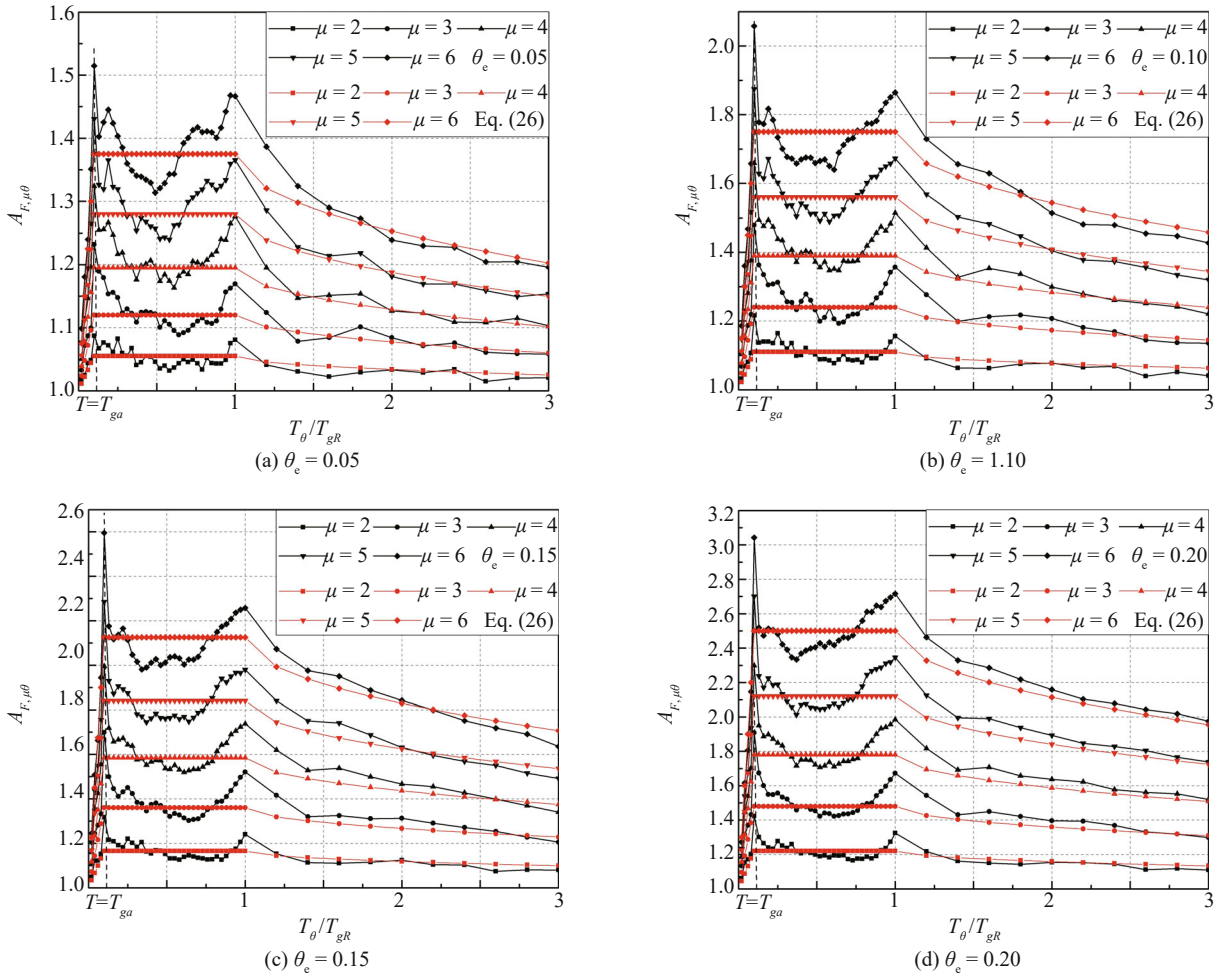

Fig. 9 The amplification factor $A_{F,\mu\theta}$ median spectra for SDOF systems and fitting curves

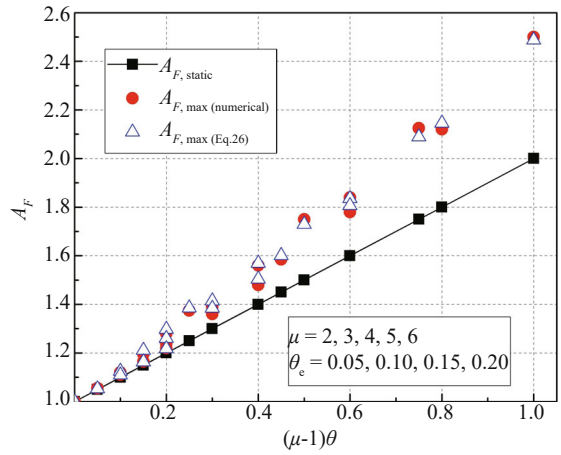

Fig. 10 Comparison of $A_{F,\ \text{static}}$ and $A_{F,\ \text{max}}$

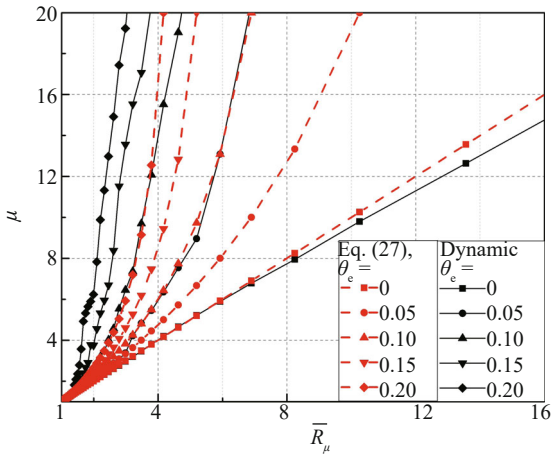

Fig. 11 The ductility response with the P-Δ effect

post-stiffness of the system can counteract the adverse influence of the $P-\Delta$ effect.

Models with the post-yield stiffness factor $\alpha=0.1$ are analyzed and the stability coefficients are $\theta_e=0$, 0.10, 0.15 and 0.2, respectively. Figure 12 presents the spectra of $R_{\mu,\alpha=0.1}$. When compared to Fig. 8, the following conclusions can be drawn:

(1) $R_{\mu,\alpha=0.1}$ are greater than $R_{\mu,\alpha=0.005}$ for the same θ_e, and significantly greater when $\theta_e>0.15$;

(2) As shown in Fig. 12(b)–12(d), $R_{\mu,\alpha=0.1}$ for $\theta_e-\alpha=0$, 0.05 and 0.1 are smaller than $R_{\mu,\alpha=0.005}$ in Fig. 8(a)–8(c) for $\theta_e=-0.005$, 0.045 and 0.095 when $T<2T_{gR}$, especially in the short period range. For $\mu=2$, or for longer period $T>2T_{gR}$, the differences between Fig. 12(b)–12(d) and Fig. 8(a)–8(c) are small.

Figure 13 give the spectra of $A_{F,\alpha=0.1}$:

$$A_{F,\alpha=0.1}=(1-\theta_e)\cdot\left(\frac{R_{\mu,\theta_e}(T_\theta/T_{gR})}{R_{\mu,\theta_e=0}(T_\theta/T_{gR})}\right)_{\alpha=0.1} \tag{28}$$

Comparing Fig.13(a), 13(b), 13(c) with Figs. 9(b), (c), (d), one can find that $A_{F.\alpha=0.1}<A_{F.\alpha=0.005}$, Fig. 13(d) illustrates the ratio $A_{F.\alpha=0.1}/A_{F.\alpha=0.005}$ for $\theta_e=0.20$. As the ductility coefficient increases, this ratio is smaller, implying that the beneficial effect of post-stiffness is more pronounced for the larger ductility factor.

Figure14 presents the following ratios:

$$\begin{aligned} r_{\theta_e-\alpha=0.05}&=\frac{A_{F,\alpha=0.1}(\theta_e=0.15)}{A_{F,\alpha=0.005}(\theta_e=0.05)},\\ r_{\theta_e-\alpha=0.1}&=\frac{A_{F,\alpha=0.1}(\theta_e=0.2)}{A_{F,\alpha=0.005}(\theta_e=0.1)} \end{aligned} \tag{29}$$

They are always greater than 1.0. This means that although the post-yield stiffness is beneficial for improving earthquake-resistant behavior and this beneficial effect is more pronounced if the ductility factor is larger, it is unable to cancel the unfavorable influences of the same amount of the stability coefficient as is the case with negative stiffness.

5 Spectra without normalized period

Although the elastic acceleration spectra used in

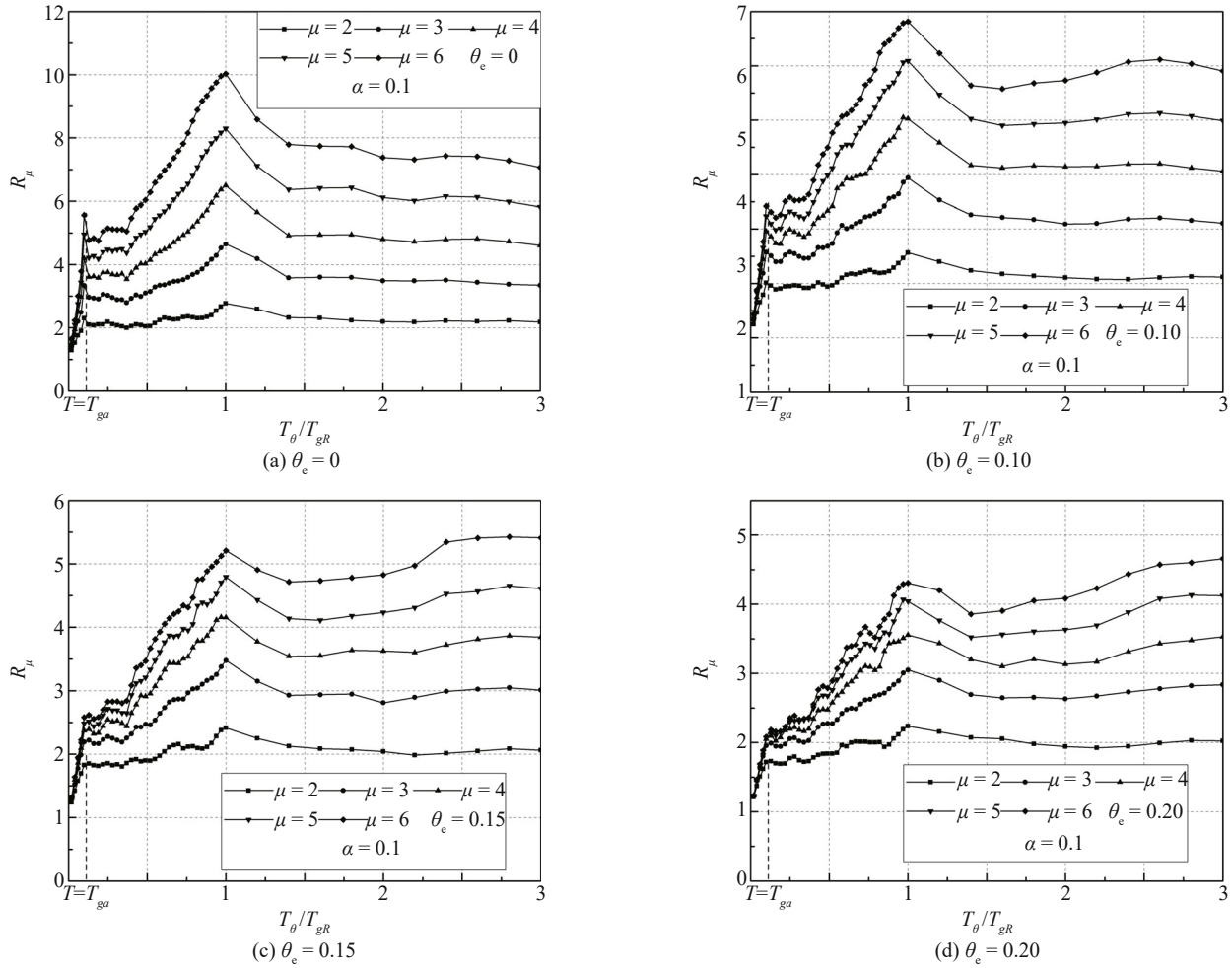

Fig. 12 The median SFRFs spectra for SDOF with a post-yield stiffness factor 0.1

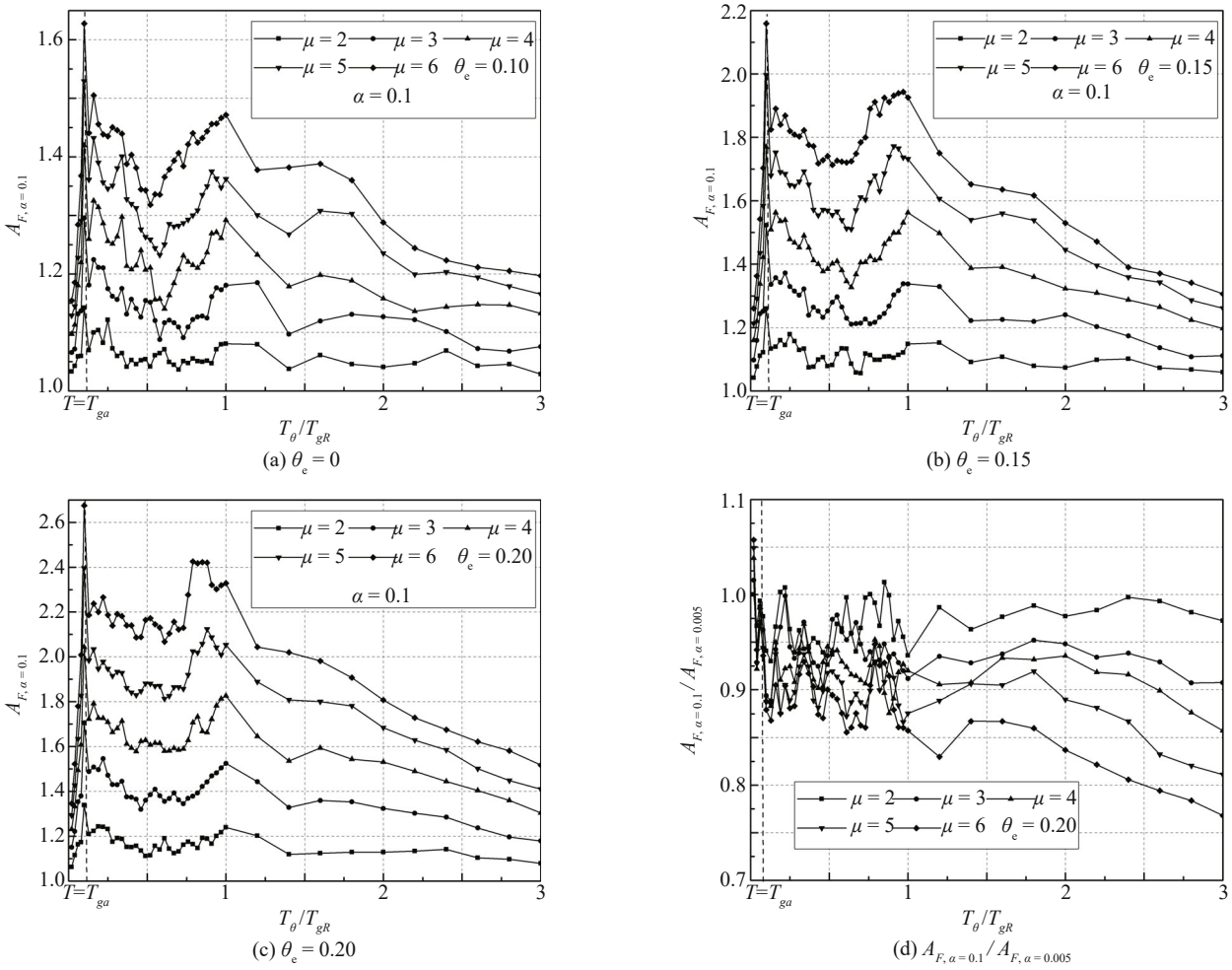

Fig. 13 The amplification factor A_F spectra for SDOF with a post-yield stiffness factor 0.1

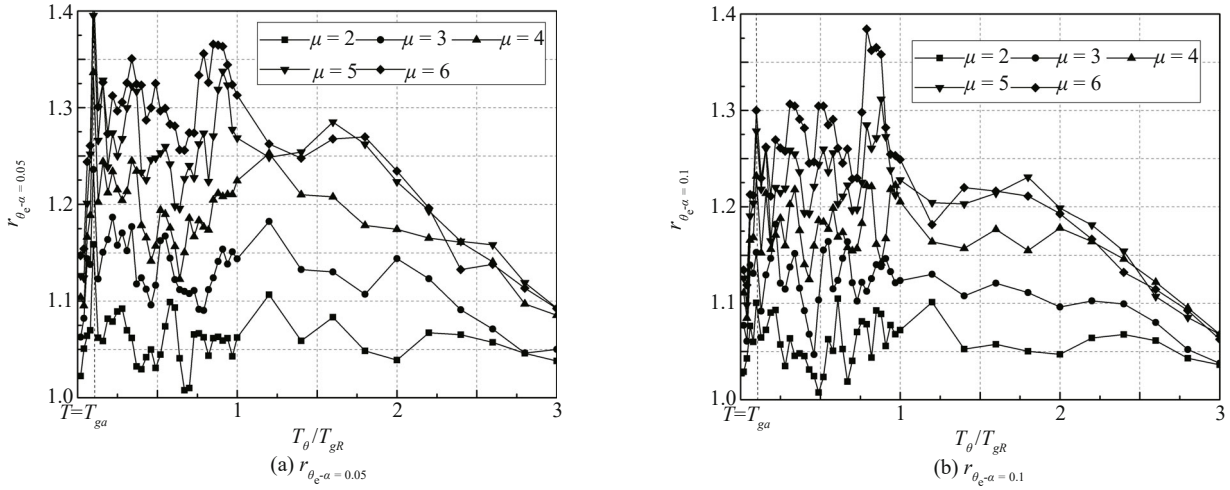

Fig. 14 The ratios of amplification factors

various codes can also be understood as normalized by two periods, as they have also two periods designated as T_C and T_D in EC8 or T_S and T_L in ASCE 7. However, they were established by directly summing up the acceleration spectral values of seismic records at the same site type. Thus, they ought to be understood as normalized by the site type, not by the period.

So, SFRFs incorporating the $P-\Delta$ effect are also established by calculating the median values of SFRFs for the 102 seismic records in site type C. The period range is 0–4 s. The results are shown in Fig. 15: the value of R_μ increases as the period varies from 0 to 0.75 s. The peak values, existing for each isolated record, disappear. As the period increases from 0.75 s, the value of R_μ

increases more slowly. R_μ approaches a constant only when $\theta_e = 0$, the equal displacement law is valid in the long period range and when there is no second order effect.

Figure 16 shows the seismic force amplification factors computed by:

$$A_{F,\mu\theta} = \frac{(1-\theta_e)\times R_{\mu,\theta_e=0}(T_\theta)}{R_{\mu,\theta_e}(T_\theta)} \tag{30}$$

At first, $A_{F,\mu\theta}$ increases rapidly from 1.0 in the range of 0–0.5 s; it reaches a maximum at $T_\theta \approx 0.75$ s. As the period increases, it decreases gradually and approaches the values of static inelastic second-order analysis. The following equation is proposed for the SFAFs in Fig.16:

$$A_{\mu\theta} = \begin{cases} 1+(A_{\max}-1)\left[\sin\left(\dfrac{2\pi}{3}T_\theta\right)\right]^{0.55+\theta_e} & (T_\theta \le 0.75 \text{ s}) \\ A_{F,\text{static}} + (A_{\max} - A_{F,\text{static}})\,\mathrm{e}^{-(2\theta_e+0.5)(T_\theta-0.75)^2} & (T_\theta > 0.75 \text{ s}) \end{cases} \tag{31}$$

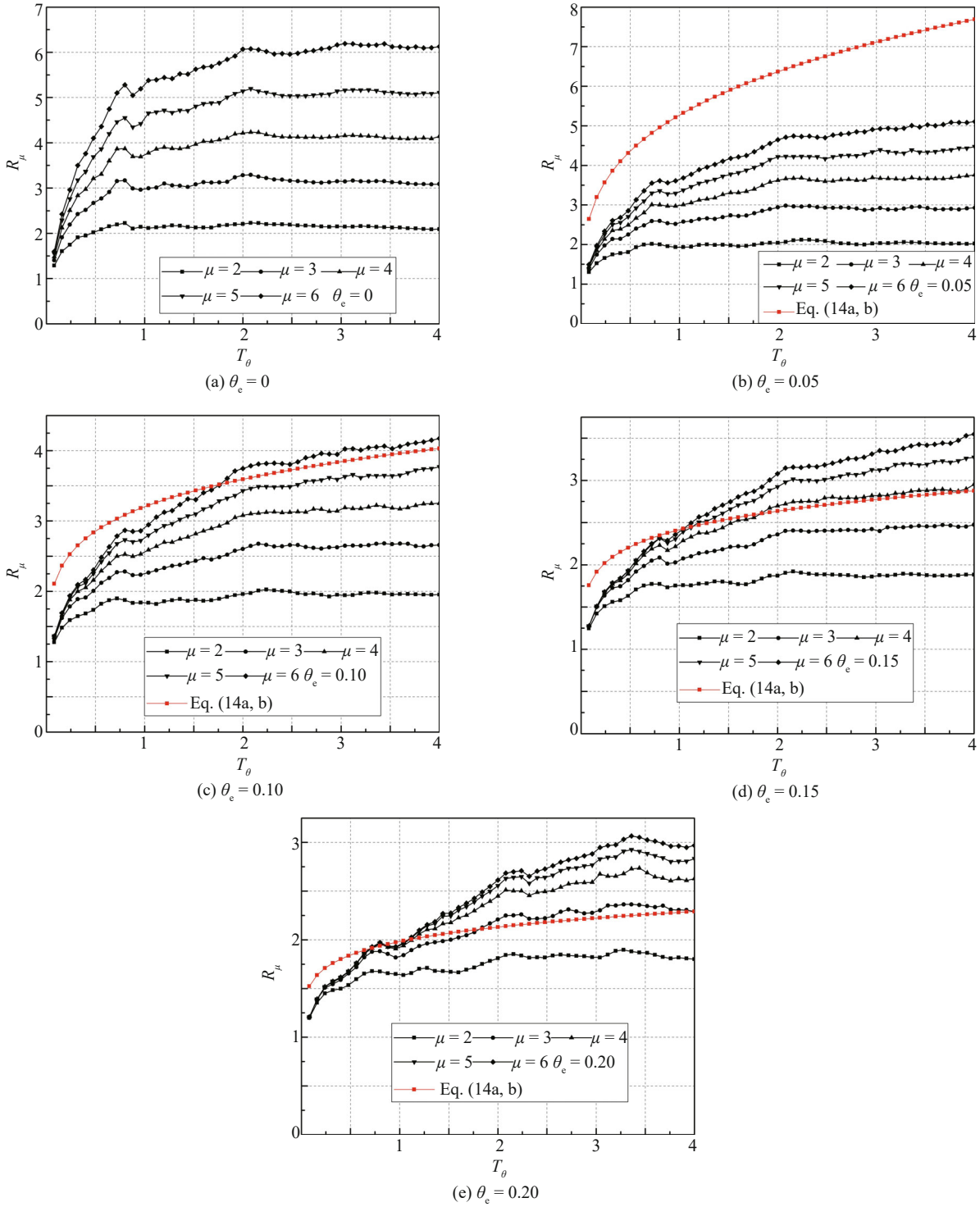

(a) $\theta_e = 0$ (b) $\theta_e = 0.05$

(c) $\theta_e = 0.10$ (d) $\theta_e = 0.15$

(e) $\theta_e = 0.20$

Fig. 15 The median SFRFs spectra for SDOF and the comparison with Adam and Jäger (2012)

where

$$A_{\max} = 1 + 1.7(\mu - 1)\theta_e \tag{32}$$

6 Comparison with available results

As shown above, the $P-\Delta$ amplification factors with normalized periods are approximately calculated, as done in Eq. (25) and Eq. (26). Note that in the practical design, the period range of the structure is usually within $T_{ga} \sim T_{gR}$; Eq. (26) is therefore adopted as the $P-\Delta$ amplification factor for comparison. For SFAF spectra without normalized periods, Eq. (32) is adopted.

After taking away the term $1/(1-\theta_e)$ from Eq. (6) by Bernal (1987), one obtains the $P-\Delta$ amplification factor as defined in this paper:

$$A_{F,\text{Bernal}} = 1 + 1.87(\mu - 1)\theta_e \tag{33}$$

Similarly, based on Eq. (7) (Wei *et al*., 2012) the $P-\Delta$ amplification factor is:

$$A_{F,\text{Wei}} = \left[1.05 + \left(2 - \frac{1}{e^{0.85(\mu-1)}}\right)\mu\theta_e\right](1-\theta_e) \tag{34}$$

According to Eq. (3) (Rosenblueth, 1965), it is:

$$A_{F,R} = \frac{1-\theta_e}{1-\mu\theta_e} \tag{35}$$

Figure 17 shows the comparison between these two results and the equations proposed in this paper. It can be seen that:

(1) Eq. (32) is larger than Eq. (26) because peak values of isolated records are included in formulating Eq. (32) statistically; Eq. (26) is the smallest among the four equations;

(2) Both Eq. (33) and Eq. (34) are slightly larger than Eq. (32);

(3) When $(\mu-1)\theta_e > 0.6$, Eq. (33) is the largest, mainly due to the fact that Bernal (1987) used the mean instead of the median values; the mean values are greater than the median ones;

(4) when $(\mu-1)\theta_e < 0.5$, Eq. (34) is larger than Eq. (33).

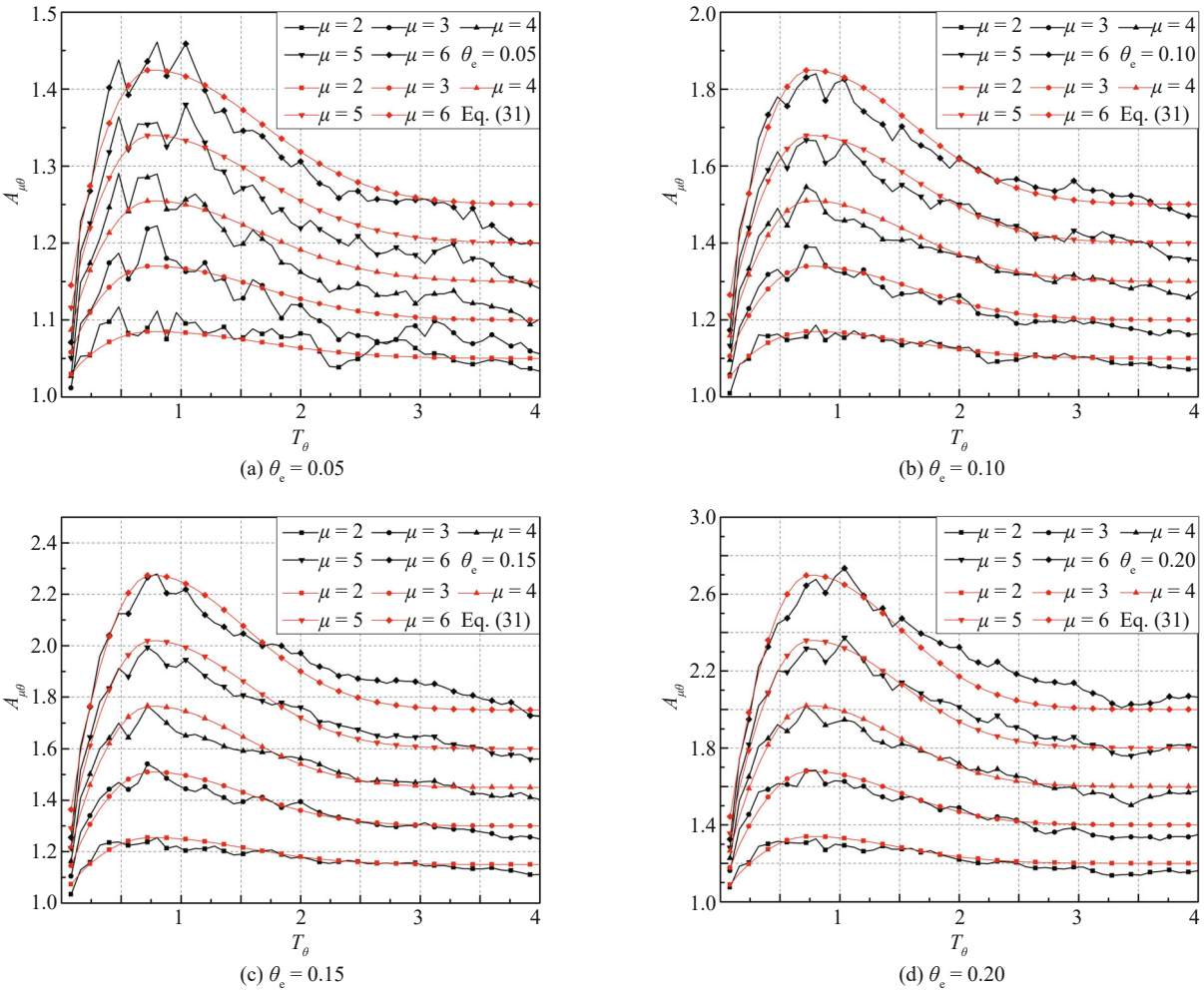

Fig. 16 The amplification factor $A_{\mu\theta}$ spectra for SDOF and fitting curves

(5) Rosenbluth's equation gives reasonable results when $(\mu-1)\theta_e \le 0.35$.

Adam and Jäger (2012) presented Eq. (14) as the collapse capacity spectrum; they did not specified a limit on the ductility factor. Therefore, their collapse capacity spectrum can be seen as the upper limit of R_μ, Eq. (14) (Adam and Jäger, 2012) are shown in Fig. 15. For $\theta_e = 0.15$ and $\theta_e = 0.2$, they are less than the results of present paper when $T_\theta > 1.5$ s and $\mu > 3$. Subsequently, a new analysis using the same 44 seismic records as those in Adam and Jäger (2012) is carried out and the results are provided in Fig.18. For $\theta_e = 0.1 \sim 0.2$, Eq. (14) is close to the upper limits of the present paper, but in the short period range, Eq. (14) is higher because of unlimited ductility. When $\theta_e = 0.15$, $T_\theta > 3$ s and $\theta = 0.2$, $T_\theta > 2.5$ s, the results in the present paper are higher

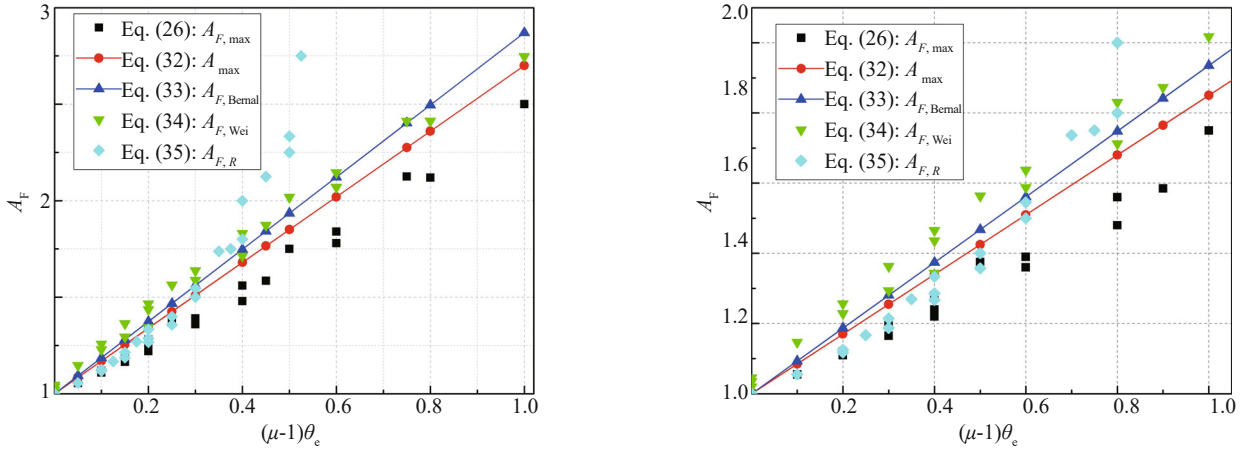

(a) $(\mu\text{-}1)\theta_e = 0\text{–}1$ (b) $(\mu\text{-}1)\theta_e = 0\text{–}0.5$

Fig. 17 Comparison with available P-Δ amplification factors

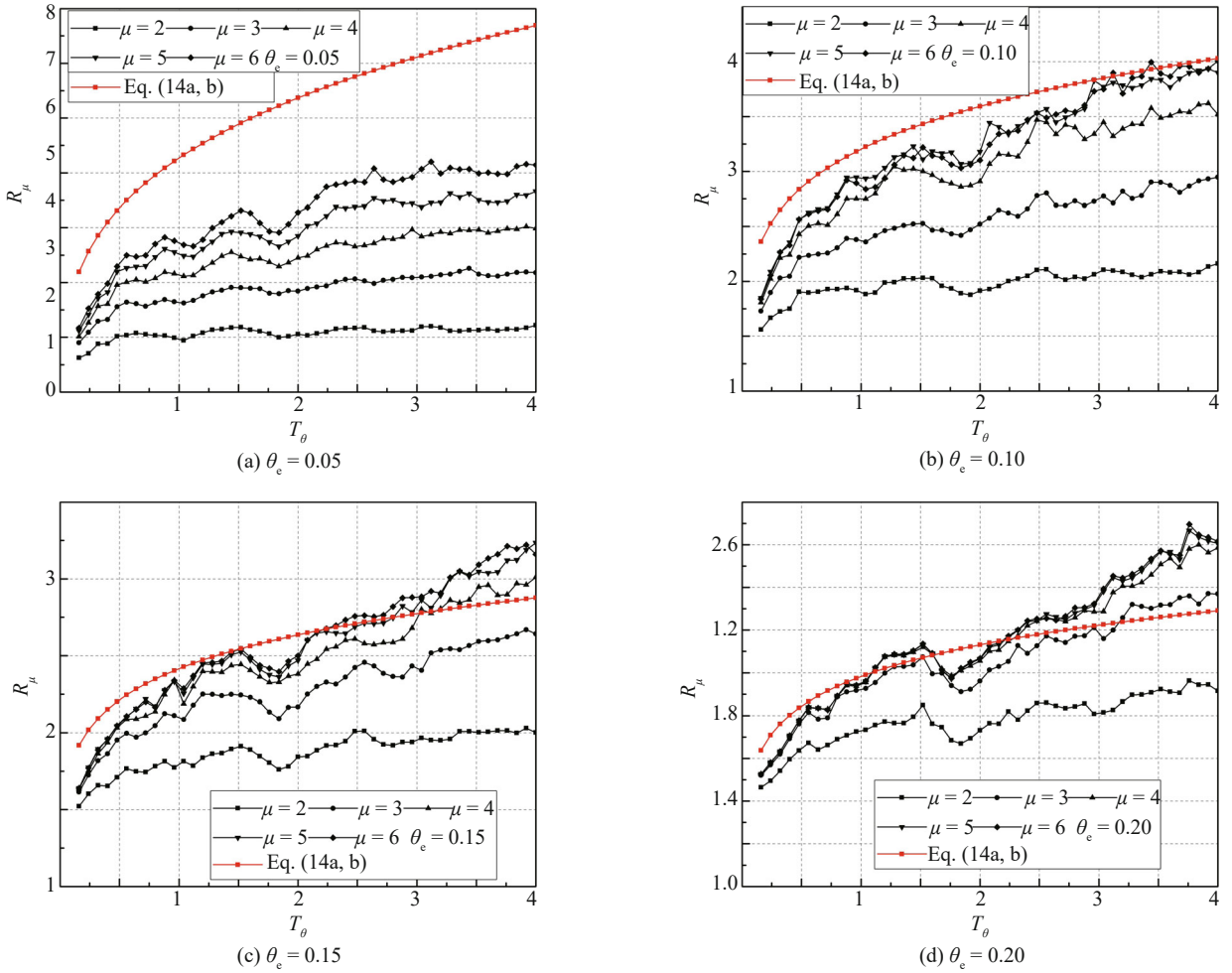

(a) $\theta_e = 0.05$ (b) $\theta_e = 0.10$

(c) $\theta_e = 0.15$ (d) $\theta_e = 0.20$

Fig. 18 The comparison of SFRFs with the collapse capacity spectra of Adam and Jäger (2012)

than Eq. (14), probably because one-story frame models (one degree of redundancy) are used in the present paper, while Adam and Jäger (2012) used an inverted pendulum (statically determinate).

7 Summary

The seismic force $P-\Delta$ amplification factors of SDOF systems were investigated. Frame models were used in the analysis, and plastic hinges were allowed at beam ends and column bases. Two ensembles of seismic records were adopted, with the first ensemble containing 102 records on site type C and the second 44 records for comparison. Two types of seismic force reduction factors spectra, and correspondingly, two types of $P-\Delta$ amplification factors were established: one type uses the natural periods normalized by two site-specific characteristic periods, T_{ga} and T_{gR} as the abscissa, while the other uses the natural periods as the abscissa. Equations for the $P-\Delta$ effect modification factors were proposed. The basic findings of this study are summarized as follows:

(1) The static inelastic $P-\Delta$ amplification factor was derived: the obtained formula is Eq. (19);

(2) The statistical distributions of SFRF spectral values were examined and found to have a lognormal distribution, so median spectra were constructed in this study;

(3) The $P-\Delta$ effect decreases the SFRFs, in particular, the peak values at the characteristic periods T_{ga} and T_{gR}. $P-\Delta$ amplification factors defined by Eqs. (23) and (30) quantify such decreases, and these definitions differ from the others in that the static elastic $P-\Delta$ amplification factor (Eq. (2)) is eliminated in this study;

(4) Equations (25) and (31) are proposed for the $P-\Delta$ amplification factors;

(5) An analysis showed that post-yield stiffness cannot fully compensate for the adverse influence of the $P-\Delta$ effect on the SFRFs for any ductility factor greater than 1.0;

(6) For two ensembles of seismic records used in this study, there exist noticeable differences among their SFRF spectra, especially when the ductility factors are greater than about 3.5;

(7) The physical meaning and application of collapse capacity spectra (with unrestricted ductility) were discussed. They were compared with the SFRF spectra with limited ductility. It was found that:

(8) The comparison of the proposed functions with available equations in the open literature has been researched.

References

Adam C and Jäger C (2012), "Seismic Collapse Capacity of Basic Inelastic Structures Vulnerable to the P-Delta Effect," *Earthquake Engineering and Structural Dynamics*, **41**(4): 775–793.

Amara F, Bosco M, Marino EM and Rossi PP (2014), "An Accurate Strength Amplification Factor for the Design of SDOF Systems with P–Δ Effects," *Earthquake Engineering and Structural Dynamics*, **43**(4): 589–611.

ASCE 7 (2010), *Minimum Design Loads for Buildings and Other Structures*, Reston: American Society of Civil Engineers.

Asimakopoulos AV, Karabalis DL and Beskos DE (2007), "Inclusion of P–Δ effect in Displacement-Based Seismic Design of Steel Moment Resisting Frames," *Earthquake Engineering and Structural Dynamics*, **36**: 2171–2188.

Bernal D (1987), "Amplification Factors for Inelastic Dynamic P–Δ Effects in Earthquake Analysis," *Earthquake Engineering and Structural Dynamics*, **15**(5): 635–651.

Bernal D (1992), "Instability of Buildings Subjected to Earthquakes," *J Struct Eng*, **118**: 2239–2260.

Borekci M, Kirçil MS and Ekiz I (2014), "Collapse Period of Degrading SDOF Systems," *Earthquake Engineering and Engineering Vibration*, **13**(4): 681–694.

Borzi B and Elnashai AS (2000), "Refined Force Reduction Factors for Seismic Design," *Engineering Structures*, **22**(10): 1244–1260.

CEN (Comité Européen de Normalisation) (2005), Eurocode 8: *Design of Structures for Earthquake Resistance. Part 1: General Rules, Seismic Actions and Rules for Buildings*.

FEMA-368 (2000), *NEHRP Recommended Provisions for Seismic Regulations for New Buildings and Other Structures Part 1: Provisions*, Washington, USA.

FEMA-440 (2005), "Improvement of Nonlinear Static Seismic Procedures," *ATC-55 Draft*, Washington, USA.

Gupta A and Krawinkler H (2000), "Behavior of Ductile SMRFS at Various Seismic Hazard Levels," *Journal of Structural Engineering*, **126**(1): 98–107.

Ibarra LF and Krawinkler HA (2005), "Global Collapse of Frame Structures Under Seismic Ex-Citations," *Report No.152*, The John A. Blume Earthquake Engineering Center.

MacRae GA (1994), "P–Δ Effects on Single-Degree-of-Freedom Structures in Earthquakes," *Earthquake Spectra*, **10**: 539–568.

Miranda E (1993), "Site-Dependent Strength-Reduction Factors," *Journal of Structural Engineering*, **119**: 3503–3519.

Miranda E and Akkar SD (2003), "Dynamic Instability of Simple Structural Systems," *Journal of Structural Engineering*, **129**(12): 1722–1726.

Miranda E and Bertero V (1994), "Evaluation of Strength Reduction Factors for Earthquake Resistant Design," *Earthquake Spectra*, **10**(2): 357–379.

Neuss CF, Maison NM and Bouwkamp JG (1983), "A Study of Computer Modelling Formulation and Special Analytical Procedures for Earthquake Response of Multistory Buildings," *A Report to the National Science Foundation*, Washington, USA.

NZS 1170.5. (2004), *Structural Design Actions, Part 5: Earthquake Actions-New Zealand*, Wellington, New Zealand, Standards New Zealand.

Ordaz M and Pérez-Rocha LE (1998), "Estimation of Strength-Reduction Factors for Elatoplastic Systems: A New Approach," *Earthquake Engineering and Structures Dynamics*, **27**(9): 889–901.

Priestley MJN, Calvi GM and Kowalsky MJ (2007), "Displacement-Based Seismic Design of Structures," IUSS Press, Pavia, Italy.

Priestley MJN, MacRae GA and Tao J (1993), "P-Delta Effect on Single Degree of Freedom Oscillators with Degrading Characteristics," *Structural Systems Research Report*, Report No. SSRP 93/05, Department of Applied Mechanics and Engineering Science, University of California, San Diego, USA.

Qu HL, Zhang JJ and Zhao JX (2011), "Strength Reduction Factors for Seismic Analyses of Buildings Exposed to Near-Fault Ground Motions," *Earthquake Engineering and Engineering Vibration*, **10**(2): 195–209.

Rosenblueth E (1965), "Slenderness Effects in Buildings," *Journal of the Structural Division*, **91**(1): 229–252.

Ucar T and Merter O (2018), "Derivation of Energy-Based Base Shear Force Coefficient Considering Hysteretic Behavior and P-Delta Effects," *Earthquake Engineering and Engineering Vibration*, **17**(1): 149–163.

Wei B, Xu Y and Li JZ (2012), "Treatment of P-Delta Effects in Displacement-Based Seismic Design for SDOF Systems," *Journal of Bridge Engineering*, **17**(3): 509–518.

Zhao YF and Tong GS (2009), "An Investigation of Characteristic Periods of Seismic Ground Motion," *Journal of Earthquake Engineering*, **13**: 540–565.